

An N/D study of the S_{11} channel πN scattering amplitude

October 18, 2021

QU-ZHI LI,[†] YAO MA,[†] WEN-QI NIU,[†] YU-FEI WANG,[‡] HAN-QING ZHENG^{♡,* ,1}

[†] *Department of Physics and State Key Laboratory of Nuclear Physics and Technology, Peking University, Beijing 100871, P. R. China*

[‡] *Institute for Advanced Simulation, Institut für Kernphysik and Jülich Center for Hadron Physics, Forschungszentrum Jülich, D-52425 Jülich, Germany*

[♡] *College of Physics, Sichuan University, Chengdu, Sichuan 610065, P. R. China*

^{*} *Collaborative Innovation Center of Quantum Matter, Beijing, Peoples Republic of China*

Abstract

Extensive dynamical N/D calculations are made in the study of S_{11} channel low energy πN scatterings, based on various phenomenological model inputs of left cuts at tree level. The subtleties of the singular behavior of the partial wave amplitude at the origin of the complex s plane are carefully analysed. Furthermore, it is found that the dispersion representation for the phase shift, δ , has to be modified in the case of πN scatterings. An additional contribution from the dispersion integral exists, which is, however, almost exactly cancelled the contribution from two virtual poles located near the end points of the segment cut induced by u channel nucleon exchanges. Relying very little on the details of the dynamical inputs, the subthreshold resonance $N^*(890)$ survives.

1 Introduction

In a series of recent publications [1] [2] [3], it is suggested that there exists a sub-threshold $1/2^-$ nucleon resonance hidden in S_{11} channel of πN scatterings, with a pole mass $\sqrt{s} = (0.895 \pm 0.081) - (0.164 \pm 0.023)i$ GeV. The result is obtained by using the production representation (PKU representation) for partial wave amplitudes [4] [5] [6] [7] [8]. It is found later that the $N^*(890)$ pole may also be generated from a conventional and simple K -matrix fit, though the latter suffers from the existence of spurious poles on 1st Riemann sheet of complex s plane [9]. Properties of $N^*(890)$ are also investigated, such as its coupling to $N\gamma$ and $N\pi$ [10, 11]. It is found that its coupling to $N\pi$ is considerably larger than that of the $N^*(1535)$, while its coupling to $N\gamma$ is comparable to that of the $N^*(1535)$. These results on couplings look reasonable and are within expectations, hence providing further evidence on the existence of $N^*(890)$.

However, to firmly establish the existence of such a subthreshold resonance is still a difficult task. Besides dispersion relations, the most frequently used tools at hand are perturbation chiral amplitudes and their unitarizations (For a recent review, see Ref. [12]), or (unitarized) resonance models. However, these unitarization techniques are far from being perfect when used in the study of low energy strong interaction physics. Especially, when applying to partial wave amplitudes with unequal mass scatterings, extra difficulties will occur, as will be discussed at some lengths in this paper. The major difficulties arose at $s = 0$ point in s plane, where chiral expansions break down since chiral expansions and partial wave projections do not commute when $s \rightarrow 0$. The expected decoupling property of heavy resonances when their masses sent to infinity is also violated in partial wave amplitudes at $s = 0$, for a purely kinematical reason in

¹Corresponding author.

partial wave projections with unequal mass scatterings. The major task of this paper is to show how the subthreshold resonance persist, irrespective of various difficulties and uncertainties left in the input quantity – the left part of the scattering amplitude.

This paper will provide further evidences on the existence of $N^*(890)$, by directly finding a pole in the S matrix element calculated from the N/D method. Early studies on low energy πN scatterings via N/D method may be found in Ref. [13] and references therein. Nevertheless, no report on the possible existence of a subthreshold resonance is known in the literature of N/D studies, to the best of our knowledge. In our practice of N/D calculations no spurious poles on first Riemann sheet are found to emerge. Also an N/D calculation faithfully reproduces all input dynamical as well as kinematical branch point singularities. We therefore think the N/D method is rather reliable. However, the calculations in N/D studies do generate spurious branch cuts and spurious poles on the second sheet, due to the truncation of numerical integrations. Nevertheless, their effects can be evaluated to see that the sum of hazardous contributions be negligible in many cases.

This paper is organized as follows: section 1 is the introduction. In section 2 a brief introduction to the N/D method is given with a solvable toy model calculation. Also in section 2 we afford a review on the production representation which is found very illuminating in understanding the complicated N/D calculations. A subtlety occurs when using the production representation in dealing with πN scatterings: the dispersion representation for the background contribution to the phase shift has to be modified, an additional contribution emerges which is however cancelled almost exactly by contributions from two virtual poles located near the end points of the cut caused by u channel nucleon pole exchanges. We put all the related discussions with respect to the subtlety in the appendix. Section 3 focuses on the singularity structure of partial wave amplitudes at $s = 0$, including the discussion on why chiral expansions break down here, and on how high energy contributions enter through an analysis on regge asymptotic behavior of $T(s)$ when $s \rightarrow 0$. Section 4 devotes to numerical analyses on how can a subthreshold resonance emerge under various phenomenological inputs.

2 The N/D recipe, a prelude

2.1 A brief introduction to N/D method

The partial wave T matrix element is expressed as

$$T = N/D , \quad (1)$$

where D contains only the s -channel unitarity cut or the right hand cut R , whereas N only contains the left hand cut (*l.h.c.*) or L . See Fig. 1, $R = [s_R, +\infty)$ whereas L represents all branch cuts except R in Fig. 1. In section 3.2 we will briefly review on how to determine the cut structure in Fig. 1 [14].

Partial wave unitarity in single channel approximation

$$\text{Im}_R T(s) = \rho(s) |T(s)|^2 , \quad (2)$$

where

$$\rho = \sqrt{(s - s_L)(s - s_R)}/s \quad (3)$$

with $s_L = (m_N - m_\pi)^2$, $s_R = (m_N + m_\pi)^2$, leads to the following relations

$$\begin{aligned} \text{Im}_R[D(s)] &= -\rho(s)N(s) , \\ \text{Im}_L[N(s)] &= D(s)\text{Im}_L[T(s)] , \end{aligned} \quad (4)$$

and subsequential N/D equations:

$$\begin{aligned} D(s) &= 1 - \frac{s - s_0}{\pi} \int_R \frac{\rho(s')N(s')}{(s' - s)(s' - s_0)} ds' , \\ N(s) &= N(s_0) + \frac{s - s_0}{\pi} \int_L \frac{D(s')\text{Im}_L[T(s')]}{(s' - s)(s' - s_0)} ds' . \end{aligned} \quad (5)$$

Notice that when there appears circular cut in T on s plane as shown in Fig. 1, the second equation of Eq. (4) should be read as $\text{disc}[N(s)] = D(s)\text{disc}[T(s)]$. Also in the second equation

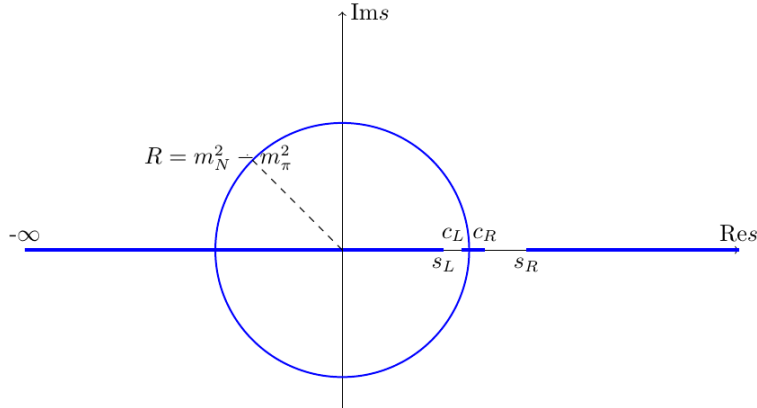


Figure 1: Branch cuts (thick blue lines) of partial wave πN elastic scattering amplitudes, where $c_L = (m_N^2 - m_\pi^2)^2/m_N^2$, $c_R = m_N^2 + 2m_\pi^2$.

of Eq. (5), when the integration is performed on the circular cut which belongs to a subset of L , $\text{Im}_L[T(s)]$ should be replaced by $\frac{1}{2i} \text{disc}[T(s)]$. After getting a numerical solution of Eq. (5), analytical continuation to the complex plane is straightforward: taking s to be complex while evaluating the integration in Eq. (5) when s is in the first sheet, and taking

$$D^{\text{II}}(s) = D(s) + 2i\rho N(s), \quad N^{\text{II}}(s) = N(s), \quad (6)$$

when s lies on the second sheet. In Eq. (5), the left cut of the partial wave T matrix element, $\text{Im}_L T$ is an input quantity. Throughout this paper, we only discuss $\text{Im}_L T$ extracted from tree level amplitudes. Hence, except in the case with t -channel ρ exchange as discussed in section 4.2, where an arc cut in s plane will be met, L is always on the real axis. For example, for pure tree level chiral amplitudes, $L = (-\infty, 0] \cup [c_L, c_R]$. We will make a rather detailed discussion on how to determine $l.h.c.s$ in section 3.2.

To solve the integral equations one may substitute D into the second equation of Eq. (5) to get

$$N(s) = N(s_0) + \tilde{B}(s, s_0) + \frac{s - s_0}{\pi} \int_R \frac{\tilde{B}(s', s)\rho(s')N(s')}{(s' - s_0)(s' - s)} ds', \quad (7)$$

with

$$\tilde{B}(s', s) = \frac{s' - s}{2\pi i} \int_L \frac{\text{disc}T(\tilde{s})}{(\tilde{s} - s)(\tilde{s} - s')} d\tilde{s}, \quad (8)$$

and use the inverse matrix method to obtain a numerical solution. Throughout this paper, we set $s_0 = 1 \text{ GeV}^2$, a value a little bit below the elastic threshold s_R .

As we will see later in this paper, there exists a subtlety when using Eq. (5) to discuss un-equal mass scatterings. The problem comes from a singularity at $s = 0$ in the partial wave amplitude and in its left cut, which stems from high energy region $t \rightarrow +\infty$ through partial wave projections, and from relativistic spin kinematics as well. But before dealing with this problem, we are more eager in finding a solution of Eq. (5) in a simplified toy model, in the following subsection.

2.2 A toy model calculation

In N/D recipe the input quantity is $\text{Im}_L T$. Let us begin with a simple version of N/D study by assuming $\text{Im}_L T$ being simulated by a set of Dirac δ functions, or equivalently

$$N = \sum_i \frac{\gamma_i}{s - s_i}, \quad (9)$$

which is to be used in the first equation of Eq. (5). I.e., there is no need for a subtraction in the second equation of Eq. (5). The T matrix in such a situation is analytically solvable. We

(arbitrarily) choose *Case I*: one pole at $s_1 = 0$, and *Case II*: one pole at $s_1 = -m_N^2$, and fit to the “data” obtained from the solutions of Roy Steiner equations [15] by tuning the parameter γ_1 , and search for poles on the s -plane. Both cases give a good fit to the data, and a sub-threshold pole emerges in each case with a location listed in Table 1. The phase shift and its PKU

	<i>Case I</i>	<i>Case II</i>
s_1	0	$-m_N^2$
γ_1 (GeV ²)	0.79	1.34
$\sqrt{s_{pole}}$ (GeV)	0.810 - 0.125i	0.788 - 0.185i

Table 1: Subthreshold pole locations using input Eq. (9).

decomposition [4] [5] are plotted in Fig. 2. On the left of Fig. 2, we see the familiar picture that the background cut contribution to the phase shift is concave and negative while the subthreshold resonance pole provides a positive and convex phase shift above threshold to counterbalance the former contribution, and the sum of the two reproduces the steadily rising phase shift data. In order to have a better understanding of this phenomenon, a brief introduction to the production representation of partial wave elastic scattering S matrix element is needed.

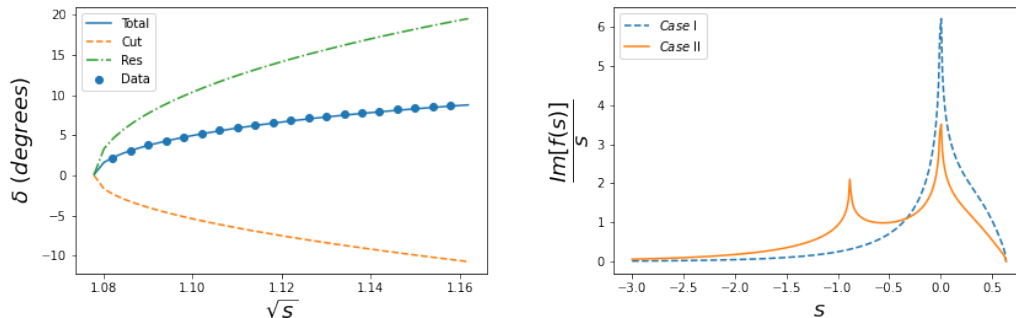


Figure 2: left: fit to the S_{11} channel πN scattering phase shift data, taking *Case II* as an example (data from Ref. [15]); right: the spectral function $\text{Im}_L f(s)/s$ of *Case I* and *II*. Notice that the singularity at $s = 0$ in *Case II* is due to the kinematical singularity in $\rho(s)$ defined in Eq. (3) rather than dynamical. For the definition of different contributions to the phase shift, one is referred to Sec. 2.3.

2.3 The PKU representation

The “spectral” function drawn on the *r.h.s.* of Fig. 2 is defined as following:

$$f(s) = \frac{s}{2i\pi} \int_L ds' \frac{\text{disc}_L f(s')/s'}{(s' - s)} + \frac{s}{2i\pi} \int_R ds' \frac{\text{disc}_R f(s')/s'}{(s' - s)}, \quad (10)$$

$$\text{disc}_{L,R} f(s) = \text{disc}_{L,R} \left(\frac{\ln S(s)}{2i\rho(s)} \right), \quad (11)$$

where the partial wave S matrix element $S = 1 + 2i\rho T$ and ρ is the kinematic factor. In Eq. (10), the integration domain is depicted in Fig. 1, it is noticed that $R = [(m_N + m_\pi)^2, +\infty)$ but actually the integrand vanishes in the elastic region, or in other words, R starts from first inelastic threshold. Elastic partial wave S matrix elements satisfy a production representation like follows:

$$S = \prod_i S_i \times e^{2i\rho(s)f(s)}. \quad (12)$$

Detailed discussions on how to obtain Eq. (12) can be found in Refs. [4] [5]. The production representation exhibits some nice features which are very useful in our analyses. One advantage

is that phase shifts from different sources are additive, i.e.,

$$\delta(s) = \sum_i \delta_i + \delta_{cut} , \quad (13)$$

where δ_i comes from the i -th pole contribution described by S_i in Eq. (12). For a resonance located at z_0 (z_0^*) it is

$$\delta_{res} = \arctan \left[\frac{\rho(s)sG[z_0]}{M^2(z_0) - s} \right] \quad (S_R = e^{2i\delta_R}) , \quad (14)$$

with $G(z_0) = \text{Im}[z_0]/\text{Re}[z_0\rho(z_0)]$ and $M^2(z_0) = \text{Re}[z_0] + \text{Im}[z_0]\text{Im}[z_0\rho(z_0)]/\text{Re}[z_0\rho(z_0)]$. For a virtual state located at s_0 ($s_L < s_0 < s_R$), its contribution is

$$\delta_v = \arctan \left[\frac{\rho(s)s}{s - s_L} \sqrt{\frac{s_0 - s_L}{s_R s_0}} \right] \quad (S_v = e^{2i\delta_v}) . \quad (15)$$

For a bound state, the above expression changes sign, i.e., $\delta_b = -\delta_v$ ($S_b = e^{2i\delta_b}$). The last contribution in Eq. (13), i.e., the background contribution to the phase shift, is

$$\delta_{cut} = \rho(s)f(s) , \quad (16)$$

with function $f(s)$ defined in Eq. (10).

The above description of the production representation only repeats what have been established in the literature. In our study of πN scatterings, however, an unexpected new phenomenon occurs. Simply speaking, the cut structure of the background phase shift, $\delta_{b.g.}$, has to be modified, due to the presence of the u -channel nucleon exchange.² As a result, an additional contribution exists in the expression of $\delta_{b.g.}$, which is, however, almost exactly cancelled by the contributions from two newly found virtual poles located near the end points (i.e., c_L and c_R defined in Fig. 1) of the segment cut induced by the u channel nucleon exchange. Since the explanation is rather lengthy, we postpone the discussions in the appendix.

The property that the phase shift contributions are additive is vital in tracing the physical origin of the phase shift. As having been stressed repeatedly, the positive value of $\text{Im}_L f(s)/s$ guarantees that the background contribution to the phase shift be negative and concave, and hence an isolated singularity on the second sheet is needed to take charge of the steady rise of near threshold phase shift. The circular cut caused by t -channel exchanges and the u -channel cut (combined with effects of two virtual poles) are not considered yet here, nevertheless they are numerically small as comparing with the cut lying on $(-\infty, s_L]$.³ Hence a large and positive $\text{Im}_L f(s)/s$ at $s = 0$, looks important as suggested in Fig. 2. The strong enhancement of $\text{Im}_L f(s)/s$ at $s = 0$ is due to two reasons: one is from the kinematic singularity at $s = 0$ from Eq. (3), the other is from the possible singularity in $T(s)$ when $s \rightarrow 0$. An example for the former is fit *Case II* in section 2.2 where $T(0) \sim \text{constant}$, while the latter example is provided by fit *Case I* where $T(s) \sim O(s^{-1})$ when $s \rightarrow 0$. In general, making use of the property of real analyticity for S matrix elements, one recasts $\text{Im}_L f(s)$, when s lies on the real axis, as $-\ln |S(s)|/2\rho(s) = -\ln [1 - 4\rho(s)\text{Im}_L T(s) + 4\rho(s)^2|T|^2]/4\rho(s)$. Hence if $T(s)$ does not vanish when $s \rightarrow 0$, then $\ln |S(s)|$ diverges logarithmically, since $\rho(s) \propto s^{-1}$ at origin. It may be worth stressing that the singularities caused by relativistic kinematics truly exist and bring physical consequences, since they enter the physical equations such as Eq. (2). A good example to realize this comes from figure 5 and Eq. (55) of Ref. [7]: without the kinematical singularity the data curve can simply not be explained.

On the other side, the inelastic right hand cut contribution to the phase shift in Eq. (10) should always be positive [3], since in that region $|S(s)| = \eta < 1$, with η the inelasticity parameter. In N/D calculations, a cutoff to the integral interval has to be adopted, i.e., $[s_R, +\infty)$ to be replaced by $[s_R, \Lambda_R^2]$. In this situation, it is not difficult to understand that the truncated N/D integration actually violates unitarity by introducing a spurious branch cut starting from $s = \Lambda_R^2$, in the sense that the effective η parameter exceeds unity: $|S(s)|^2 = [1 - 4\rho(s)\text{Im}_R T(s) + 4\rho(s)^2|T|^2] = [1 + 4\rho(s)^2|T|^2] > 1$, when $s > \Lambda_R^2$, since a truncation implies actually $\text{Im}_R T = 0$. So one has to be cautious when performing the N/D calculations by

²The cut structure of $S_{b.g.} = \exp 2i\rho f(s)$ remains unchanged, as it should.

³Previous examples can be found in Refs. [4] [1] [9].

monitoring to what extent unitarity is violated. This may be fulfilled at quantitative level by, for example, calculating the contribution from the region above Λ_R^2 to the phase shift, through Eq. (10). It is found that, when doing calculations in this paper, the violation can either be large or small, depending on whether or not the input quantity $T_L(s)$ at $s = \Lambda_R^2$ is too large or small. For the former, an example is the χ PT input which is not valid anymore at $\Lambda_R^2 = 1.48 \text{ GeV}^2$, i.e., the value we choose in most of our calculations. However, the $N^*(890)$ exists with a rather stable location, irrespective to the pollution of truncation of integration.

Encouraged by the discussions made in section 2.2, we plan to make a more realistic N/D calculation at next steps. The first thing needs to be settled down is of course choosing an input $\text{Im}_L T$ as much realistic as possible. One may choose the χ PT outputs as an input here, as what is adopted in Refs. [1] [2] [3]. A careful analysis reveals, however, that the partial wave projection of χ PT amplitudes encounters a rather severe problem at $s = 0$. In the following section we dedicate to the study of such a problem.

3 The singularity structure of $T(s)$ at $s = 0$

As suggested in the end of the above section, to make a more realistic calculation, one may use χ PT amplitudes to extract $\text{Im}_L T$ [3]. However, the results may not be directly applicable to Eq. (5), and should be treated with great care. The integration interval for $N(s)$ is $L = (-\infty, 0]$ for tree level estimation here. The $\mathcal{O}(p^3)$ level $\text{Im}_L T$ behaves as $\mathcal{O}(s^{-7/2})$ when $s \rightarrow 0$, and at $\mathcal{O}(p^2)$ level it behaves as $\mathcal{O}(s^{-5/2})$, while from a rather general argument to be discussed in section 3.2 these strong singularities at $s = 0$ are not physical. Hence one has to find a way to get rid of these artifacts caused by partial wave projections of χ PT amplitudes.

In general, singularities of the partial wave T matrix element at $s = 0$ come from two aspects:

- the $\mathcal{O}(p^n)$ ($n \geq 2$) level χ PT amplitudes behave as $s^{-n-1/2}$ when $s \rightarrow 0$ for unequal mass scatterings, after partial wave projections, and the integer n increases when the chiral order increases.
- the left-hand cut around $s = 0$ receives singular contribution from high energy region of crossed channels, i.e., $t, u \rightarrow \infty$, through partial wave projections;

We will address these problems in some details below. It is worth pointing out beforehand, that though in N/D approach one has to deal with these problems cautiously, the calculations made in Refs. [3] and [1] are luckily insensitive to the problem. Though the background contribution to the phase shift will be enhanced incorrectly by the contribution in the vicinity of $s = 0$, it will be largely compensated by tuning the cutoff parameter Λ_L^2 when evaluating the *l.h.c.* integral. More interestingly even though the integral of $f(s)$ is enhanced near $s = 0$, its derivatives behave very differently. For example,

$$\frac{df(s)}{ds} = -\frac{1}{\pi} \int ds' \frac{\ln |S(s')|/2\rho(s')}{(s' - s)^2}. \quad (17)$$

Now the integrand near $s' = 0$ behaves like $\sim s' \ln s'$ and the unwanted singularity is killed. This fact may be translated into a more transparent language: in Refs. [3] [1], except the scattering length which anyway needs to be fitted by tuning Λ_L^2 , the other quantities such as the curvature of the phase shift curve are quite immune to the disease infected from $s = 0$.

3.1 Artificial singularities in partial wave χ PT amplitudes

We notate the process as $N(p, \sigma) + \pi(q) \rightarrow N(p', \sigma') + \pi(q')$, where p, q, p', q' are the momenta and σ, σ' are the spins. The Mandelstam variables are

$$s = (p + q)^2 = (p' + q')^2, \quad t = (p - p')^2 = (q - q')^2, \quad u = (p - q')^2 = (p' - q)^2. \quad (18)$$

The full amplitude, \mathcal{T} , can be decomposed as (the following discussions are all for isospin $I = 1/2$ only),

$$\mathcal{T} = \bar{u}(p', \sigma') \left[A(s, t) + \frac{\not{q} + \not{q}'}{2} B(s, t) \right] u(p, \sigma). \quad (19)$$

The results of the scalar functions A, B are for example listed in Refs. [1,3] (further references are found in Refs. [16] [17] [18] [19] [20] [21]). From $\mathcal{O}(p^2)$ on, the χ PT lagrangian contains 4-point $\pi\pi NN$ contact terms, which contributes to the scalar functions as (C refers to constants),

$$A[\mathcal{O}(p^2)] \supset C(s-u)^2, \quad A[\mathcal{O}(p^3)] \supset C(s-u)^3. \quad (20)$$

More explicitly,

- at $\mathcal{O}(p^1)$ (Born and contact diagrams):

$$\begin{aligned} A_1 &= \frac{g^2 m_N}{F^2}, \\ B_1 &= \frac{1-g^2}{F^2} - \frac{3m_N^2 g^2}{F^2(s-m_N^2)} - \frac{m_N^2 g^2}{F^2} \frac{1}{u-m_N^2}; \end{aligned} \quad (21)$$

- at $\mathcal{O}(p^2)$ (only contact diagram):

$$\begin{aligned} A_2 &= -\frac{4c_1 m_\pi^2}{F^2} + \frac{c_2(s-u)^2}{8m_N^2 F^2} + \frac{c_3}{F^2}(2m_\pi^2 - t) - \frac{c_4(s-u)}{F^2}, \\ B_2 &= \frac{4m_N c_4}{F^2}; \end{aligned} \quad (22)$$

- at $\mathcal{O}(p^3)$ (Born diagram):

$$\begin{aligned} A_{3B} &= -\frac{m_N g}{F^2} \times 4m_\pi^2(d_{18} - 2d_{16}), \\ B_{3B} &= \frac{4m_\pi^2 g(d_{18} - 2d_{16})}{F^2} \times \frac{su + m_N^2(2u - 3m_N^2)}{(s-m_N^2)(u-m_N^2)}; \end{aligned} \quad (23)$$

- at $\mathcal{O}(p^3)$ (contact diagram):

$$\begin{aligned} A_{3C} &= -\frac{(d_{14} - d_{15})(s-u)^2}{4m_N F^2} + \frac{(d_1 + d_2)}{m_N F^2}(s-u)(2m_\pi^2 - t) \\ &\quad + \frac{d_3}{8m_N^3 F^2}(s-u)^3 + \frac{4m_\pi^2 d_5}{m_N F^2}(s-u), \\ B_{3C} &= \frac{(d_{14} - d_{15})(s-u)}{F^2}. \end{aligned} \quad (24)$$

In the expressions above, g is the axial-vector coupling constant, F is the pion decay constant, and c_i, d_i are low-energy constants.

The partial wave projection is done on helicity amplitudes:

$$\begin{aligned} \mathcal{T}_{++} &= \sqrt{\frac{1+z_s}{2}} [2m_N A(s, t) + (s - m_\pi^2 - m_N^2)B(s, t)], \\ \mathcal{T}_{+-} &= \sqrt{\frac{1-z_s}{2s}} [(s - m_\pi^2 + m_N^2)A(s, t) + m_N(s + m_\pi^2 - m_N^2)B(s, t)], \end{aligned} \quad (25)$$

where $z_s = \cos\theta$, and θ is the scattering angle; T_{++} stands for that the helicities of the initial and final nucleon are both $+1/2$, while T_{+-} means the final nucleon has helicity $-1/2$. The relations between the Mandelstam variables and the scattering angle ($z_s = \cos\theta$) are:

$$t(s, z_s) = 2m_\pi^2 - \frac{(s + m_\pi^2 - m_N^2)^2}{2s} + \frac{[s - (m_\pi + m_N)^2][s - (m_\pi - m_N)^2]}{2s} z_s, \quad (26)$$

$$u(s, z_s) = m_\pi^2 + m_N^2 - \frac{s^2 - (m_\pi^2 - m_N^2)^2}{2s} - \frac{[s - (m_\pi + m_N)^2][s - (m_\pi - m_N)^2]}{2s} z_s. \quad (27)$$

The S_{11} amplitude is from $J = 1/2$ partial wave helicity amplitudes:

$$\begin{aligned} T_{++}^J &= \frac{1}{32\pi} \int_{-1}^1 dz_s \mathcal{T}_{++}(s, t(s, z_s)) d_{1/2, 1/2}^J(z_s), \\ T_{+-}^J &= \frac{1}{32\pi} \int_{-1}^1 dz_s \mathcal{T}_{+-}(s, t(s, z_s)) d_{-1/2, 1/2}^J(z_s), \end{aligned} \quad (28)$$

where d stands for Wigner small- d matrix. For S_{11} channel,

$$T(S_{11}) = T_{++}^{J=1/2} + T_{+-}^{J=1/2} . \quad (29)$$

From this formula the singularity at $s = 0$ is obvious. On the one hand, in Eq. (25) the kinematic effects give an $s^{-1/2}$ factor, which makes $s = 0$ a branch point. On the other hand, see for example in Eq. (24), contact terms from χ PT expansions lead to higher and higher order polynomials of $s - u$:

$$\mathcal{T}[\mathcal{O}(p^n)] \supset C(s - u)^n . \quad (30)$$

According to Eq. (27), $u(s \rightarrow 0) \rightarrow s^{-1}$, so when $n \geq 2$

$$\mathcal{T}[\mathcal{O}(p^n)](s \rightarrow 0) \sim C s^{-n-1/2} , \quad (31)$$

where the extra factor $-1/2$ in the power comes from kinematic effects of helicity basis. Eq. (31) indicates that the higher order of χ PT calculation is employed, the stronger singularity will occur near $s = 0$ and the chiral series breaks down. Apparently this is only an artificial problem caused by chiral expansions since it contradicts the genuine singularity structure expected when $s \rightarrow 0$, as discussed in the end of section 3.2: the Froissart bound forbids a power behavior like Eq. (31) when $s \rightarrow 0$. In principle one would not hope Eq. (31) to appear in the expression of $\text{Im}_L T$ when using N/D .

3.2 High energy contributions from crossed channels

One writes a spectral representation of the partial wave amplitude [14], for t -channel:

$$T \sim \int_{\sigma_t}^{+\infty} dt' \Sigma(s, t') \int_{-1}^1 d \cos \theta \frac{R(\cos \theta)}{t - t'} , \quad (32)$$

where Σ is the Mandelstam spectral function, $\sigma_t = 4m_\pi^2$ is the threshold of t -channel process, and R is the basis function of the partial wave projection (usually the linear combinations of Wigner- d matrices). The function R can be expanded at $t = t'$: $R = R_0 + (t - t')R_1 + \dots$, and only the leading order causes singularities:

$$T \propto \int_{\sigma_t}^{+\infty} dt' \Sigma(s, t') \beta^{-1} \ln \left[\frac{\alpha + \beta}{\alpha - \beta} \right] , \quad (33)$$

with

$$\alpha = t' - 2m_\pi^2 + \frac{(s + m_\pi^2 - m_N^2)^2}{2s} , \quad \beta = \frac{[s - (m_\pi + m_N)^2][s - (m_\pi - m_N)^2]}{2s} . \quad (34)$$

Therefore the left-hand cut is described by the equation

$$\alpha^2 = \beta^2 ; \quad (35)$$

which gives

$$s_\pm(t') = m_\pi^2 + m_N^2 - \frac{t'}{2} \pm \frac{1}{2} \sqrt{(t' - 4m_\pi^2)(t' - 4m_N^2)} . \quad (36)$$

When t' takes the value from σ_t to $+\infty$, the trajectory of this solution traces out the left-hand cut. The following conclusions can be obtained:

- when $t' \in [4m_\pi^2, 4m_N^2]$, the cut appears as a circle $\text{Re}s^2 + \text{Im}s^2 = (m_N^2 - m_\pi^2)^2$, and the endpoint to the right $s = m_N^2 - m_\pi^2$ corresponds to $t' = \sigma_t = 4m_\pi^2$;
- when $t' \in (4m_N^2, +\infty)$, s_- generates the cut $(-\infty, m_\pi^2 - m_N^2)$, and $-\infty$ corresponds to $t' \rightarrow +\infty$;
- when $t' \in (4m_N^2, +\infty)$, s_+ generates the cut $(m_\pi^2 - m_N^2, 0)$, and actually 0 corresponds to $t' \rightarrow +\infty$;

One performs a similar analysis in u -channel and the solution is

$$s_1(u') = \frac{(m_\pi^2 - m_N^2)^2}{u'}, \quad s_2(u') = 2(m_\pi^2 + m_N^2) - u'. \quad (37)$$

There is a nucleon pole $u' = m_N^2$, giving a segment cut $((m_\pi^2 - m_N^2)^2/m_N^2, 2m_\pi^2 + m_N^2)$. When $u' > \sigma_u = (m_\pi + m_N)^2$, s_1 gives $(0, (m_N - m_\pi)^2)$ and $s_1 \rightarrow 0$ just when $u' \rightarrow +\infty$; while s_2 generates $(-\infty, (m_N - m_\pi)^2)$ with $s_2 \rightarrow -\infty$ when $u' \rightarrow +\infty$.

It was pointed out in Ref. [5] that, for meson – meson scatterings, if $T(s, t) \sim O(t^n)$ when $t \rightarrow \infty$ for fixed s , then the partial wave amplitude behaves as $T(s) \sim O(s^{-n})$ when $s \rightarrow 0$. Considering the Froissart bound in the crossed channel $|T(t, \cos\theta_s = 1)| < t \ln^2 t$, it is expected that the proper singularity behavior for s -channel partial wave amplitude near $s = 0$ is no more singular than $T(s) \sim O(s^{-1})$ (up to some logarithmic corrections). This estimation can even further be improved. It is seen from the above discussions that as $s \rightarrow 0_-$, there is a high energy contribution from the $t \rightarrow +\infty$ region. In this region the full amplitude is governed by t -channel ($\pi\pi \rightarrow N\bar{N}$) reggeon exchanges. The leading Regge trajectory is $\Delta(1232)$ with the intercept parameter $\alpha_\Delta(0) \simeq 0.19$ [22], which leads to a weak singularity

$$T \sim s^{-\alpha_\Delta(0)}, \quad (38)$$

for the partial wave amplitude, when $s \rightarrow 0_-$. The $s \rightarrow 0_+$ limit is the same according to for example Ref. [22].

All the discussions given above in this section are on how to determine $l.h.c.s$ generated dynamically, or in other words, cuts originated from physical absorptive singularities from crossed channels. Besides these dynamical $l.h.c.s$ there exists an additional cut $(-\infty, 0]$ for pure kinematical reasons: the nucleon spinor wave function provides a \sqrt{s} branch cut which already showed up in the second equality in Eq. (28). The effect of branch cut singularity from relativistic kinematics truly exists, as has already been addressed in section 2.3.

4 Numerical analyses of N/D method

It has been made clear in the above section, that using χ PT inputs of $\text{Im}_L T$ encounters the problem that the partial wave projections of χ PT amplitudes lead to a strong but incorrect singularity at $s = 0$, by violating what is expected from rather general constraints of quantum field theory. Nevertheless it is not clear yet, to what extent the use of χ PT results may distort the physical output. In the following we devote to the study of this problem by invoking $\mathcal{O}(p^2)$ and $\mathcal{O}(p^3)$ (tree level amplitude only) χ PT results, since in $\mathcal{O}(p^1)$ case no free parameter is available for a data fit. Nevertheless, the $\mathcal{O}(p^1)$ N/D unitarization can still be made and compared with data, which ends up with a pole location $\sqrt{s} = 1.08 - i0.23$ GeV and a steadily rise phase shift larger than data by roughly 5 degrees at $\sqrt{s} = 1.16$ GeV.

4.1 N/D calculations using pure χ PT inputs

The singularity of $\mathcal{O}(p^2)$ $\text{Im}_L T$ when $s \rightarrow 0$ behaves as $\mathcal{O}(s^{-2-1/2})$. Which, as discussed previously, is not physical. We nevertheless still perform the N/D calculation to see what happens. In doing such a calculation it is noticed that the sick singularity behavior destroys the validity of Eq. (8). To overcome the problem, the auxiliary function \tilde{B} in Eqs. (7) and (8) can be formally written as $\tilde{B}(s, s_0) = T_L(s) - T_L(s_0)$, where T_L is taken as the $\mathcal{O}(p^1)$ partial wave amplitude (Eq. (51)) plus the $\mathcal{O}(p^2)$ part of T_{+-}^J , since at $\mathcal{O}(p^2)$ level T_{++}^J does not contribute to the imaginary part on the left. In this way we avoid the discussions on possible subtractions encountered at two endpoints of the integral defined in Eq. (8).⁴ The subtraction constant $N(s_0)$ appeared in Eq. (7), or $T(s_0)$, serves as a free fit parameter.

At $\mathcal{O}(p^2)$ level there are four low energy constants (LECs) c_i with $i = 1, \dots, 4$. There are different sets of c_i parameters found in the literature (e.g., Refs. [23], [13], [24], [25], [1]). For these LECs, certain bounds, i.e., the positivity constraints [26] are obeyed.

⁴One may redefine $T(s) = \tilde{T}(s)/s^2$ and $\tilde{T}(s) = N(s)/D(s)$ to avoid the singularity in the integral in Eq. (8) at $s = 0$. The results are similar to analyses presented in this manuscript.

A good fit is obtained with $c_1 = -0.40$, $c_2 = 3.50$, $c_3 = -3.90$, $c_4 = 2.17$, $N(s_0) = 0.47$, and the pole locates at

$$\sqrt{s} = 1.01 \pm 0.19 \text{ GeV}. \quad (39)$$

In addition, we have also employed different sets of c_i , and the results change very little. For instance when we take the central values of c_i 's from Ref. [23] (NLO): $c_1 = -0.74 \pm 0.02$, $c_2 = 1.81 \pm 0.03$, $c_3 = -3.61 \pm 0.05$, $c_4 = 2.17 \pm 0.03$ (in units of GeV^{-1}), the pole position is $0.99 - 0.16i$ GeV though the phase shift does not fit data very well. It is noticed that, the spurious branch cut becomes a bit annoying here, contributing to the phase shift at $\sqrt{s} = 1.16$ GeV roughly -6° . Nevertheless, this spurious effect is far from being dominant as can be seen from Fig. 3, where one finds the total background contribution exceeds -30° , and hence is not worrisome. It is not totally clear to us yet why and under what situation the spurious branch cut becomes numerically visible. One conjecture is that the $\mathcal{O}(p^2)$ χ PT input itself becomes sick at $\Lambda_R^2 = 1.48 \text{ GeV}^2$, hence amplifies the contribution of the spurious branch cut. Finally, since the effect generated from the cut at $s = \Lambda_R^2$ is small, we still think such type of solutions are acceptable for the evaluation of physics at lower energies.

As a comparison we plot the ‘‘spectral function’’, i.e., $\text{Im}_L f(s)/s$, obtained here together with those discussed in section 2.2, in Fig. 3. Comparing Eq. (39) with that in table 1, and different

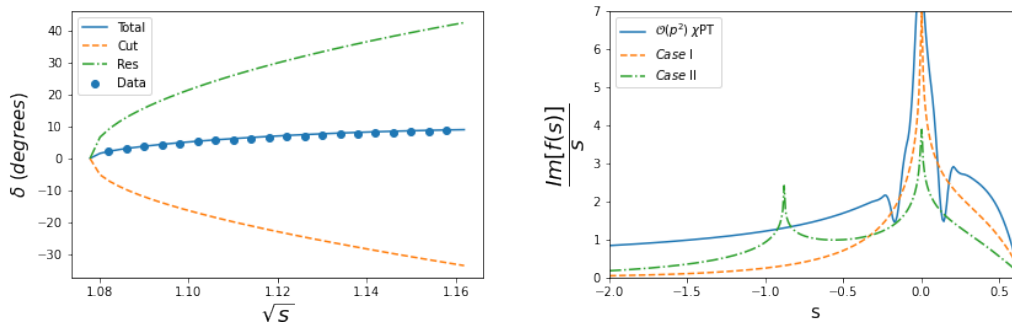


Figure 3: left: N/D fit to the S_{11} phase shift with $\mathcal{O}(p^2)$ χ PT input; right: a comparison of different $\text{Im}f(s)/s$ in different situations.

l.h.c contributions drawn in Fig. 3, we observe that the $\mathcal{O}(p^2)$ calculation overestimates the *l.h.c* contribution comparing with that of *Case II*. As a result, the pole contribution to the phase shift has to be increased and hence the pole location has to move towards to the right direction in s plane closer to the πN threshold. But of course, such discussions are only meaningful under the condition that the effects of spurious branch cut and the spurious pole around $s = \Lambda_R^2$ cancel each other.

If all the spurious contributions are ignored,⁵ then we may ask a question. The calculation here and that in Ref. [3] use the same ‘data’ sample and *l.h.c* while in Ref. [3] the pole locates at $\sqrt{s} = 0.86 \pm 0.05 - i(0.13 \pm 0.08)$ GeV. Comparing with Eq.(39) it is found that there exists a rather large systematic error in determining the pole location. One possible reason to explain this may come from the fact that in Ref. [3] a truncation of *l.h.c* is performed while in here there is no truncation on the left, see Eq. (7). In fact in the calculation made in table 4 of Ref. [3], it is found that when sending the cutoff s_c to ∞ the pole location moves upwards to $\sqrt{s} = 0.91 - i0.21$ GeV, i.e., getting closer to Eq. (39).

Finally, we have also tested the $\mathcal{O}(p^3)$ inputs (at tree level only) and found that the outputs are similar to the situation found in the $\mathcal{O}(p^2)$ case, so we no longer discuss the results here anymore.

⁵Because of two excuses: firstly they cancel each other; secondly, they are from distant places as they are associated with the cutoff at $s = \Lambda_R^2$ anyway. It is desirable to know the possible origin of spurious effects since it leaves the hope to isolate and to remove them. On the contrary, it is difficult to cure the similar problem in Padé approximation [27].

4.2 N/D calculation using phenomenological models

In the above section we have made discussions on the problem encountered when using χ PT results to estimate the *l.h.c.* The higher order terms appeared in the chiral lagrangian describing πN interactions are obtained by integrating out heavy degrees of freedom like the ρ meson in t -channel and N^* resonances in s and u -channels, etc..⁶ The ill singularities at $s = 0$ in partial wave chiral amplitudes come at least partly from integrating out heavy degrees of freedom. To see this more clearly, let us write down an effective interaction lagrangian responsible for t -channel ρ meson exchange,

$$\mathcal{L}_t = g_\rho \vec{\rho}^\mu \cdot (\partial_\mu \vec{\pi} \times \vec{\pi}) + g_\rho \bar{N} \frac{1}{2} \vec{\tau} \cdot (\gamma^\mu \vec{\rho}_\mu + \frac{\kappa}{2m_N} \sigma^{\mu\nu} \partial_\mu \vec{\rho}_\nu) N, \quad (40)$$

where g_ρ and κ are resonance coupling constants, $\vec{\tau}$ are Pauli matrices, $\vec{\rho}_\mu$, $\vec{\pi}$ and N refer to ρ resonance, pion and nucleon, respectively. For S_{11} channel, the ρ exchange contribution to the invariant amplitude, Eq. (19), can be obtained:

$$A = \frac{g_\rho^2 \kappa (u - s)}{2m_N (t - m_\rho^2)}, \quad B = \frac{2g_\rho^2 (\kappa + 1)}{t - m_\rho^2}. \quad (41)$$

Now, if a $1/m_\rho$ expansion is made, at leading order we have

$$A = \frac{g_\rho^2 \kappa (s - u)}{2m_N m_\rho^2}, \quad B = -\frac{2g_\rho^2 (\kappa + 1)}{m_\rho^2}. \quad (42)$$

Comparing with Eq. (22), we find that the ρ meson exchange only contributes to c_4 term [29]. As we already know from the discussions made in section 3.1, the c_4 term will cause an $s^{-3/2}$ singularity after partial wave projection. This is avoidable, if we do not make a $1/m_\rho$ expansion in the beginning. It can be seen that all these resonance exchange amplitudes contain singularity of $s^{-1/2}$ type at most when $s = 0$. Therefore partial wave projections and chiral expansions do not commute, which can be checked directly by evaluating t -channel ρ exchange contributions by making partial wave projections of Eqs. (25) and (28).

We further make an asymptotic expansion of the ρ exchange contributions to $T(S_{11})$ in the vicinity of $s = 0$ and find that the first two most singular terms are of type

$$\frac{a + bs}{\sqrt{s}}, \quad (43)$$

which are not of type $\mathcal{O}(s^{-5/2})$ obtained if the ρ propagator were expanded beforehand. Similar things happen if we introduce, for example, a u -channel as well as s -channel S_{11} resonance exchange. In this situation one can prove that expanding the N^* propagator in the full amplitudes leads contributions to c_3 and c_4 terms in Eq. (22). Not making a chiral expansion beforehand the resonance exchange contribution to the partial wave amplitude can be expanded at $s = 0$ and similar results as Eq. (43) are again obtained, so do the P_{11} resonance exchange contributions.

Explicit expressions for resonance contributions to parameters, e.g., a and b defined in Eq. (43) are obtainable. However, another obscure problem occurs here. These coefficients depend on the mass parameters of the exchanged resonances and do not vanish as the resonance mass gets large, which seems to contradict the general expectation from the decoupling theorem [30] [31].⁷ Without a deeper understanding on this problem, we point out that the sign of contributions from different sources can be different. For example, the t -channel ρ exchange contribution to parameter a is $a(\rho) = -\frac{g_\rho^2 \kappa (m_N^2 - m_\pi^2)}{64\pi m_N}$; the $\frac{1}{2}^+$ baryon exchange contribution is $a(N^{*+}) = \frac{(g_{N^*})^2 (-m_N^2 + m_\pi^2) (3m_N^2 + (m_{N^*})^2)}{128\pi F^2 m_{N^*}}$; whereas the $\frac{1}{2}^-$ resonance exchange contribution is $a(N^{*-}) = \frac{(g_{N^*})^2 (m_N^2 - m_\pi^2) (3m_N^2 + (m_{N^*})^2)}{128\pi F^2 m_{N^*}}$, which is different in sign as comparing with that of the first two contributions. Hence, a conspiracy theory of cancellation is assumed to overcome the problem of too large resonance contributions to parameter a , or more accurately, $T(s)$ near

⁶In the meson-meson scattering lagrangian, the LECs at $\mathcal{O}(p^4)$ level are known to be saturated by heavy degrees of freedom [28]. In meson-baryon system, systematic studies on this point are not known to the authors.

⁷The reason behind this phenomenon is that as $s \rightarrow 0$ the interval of partial wave integration diverges, make any "heavy" mass scale not heavy anymore and cannot be naively integrated out.

$s = 0$. In practice, we therefore use the $\mathcal{O}(p^1)$ χ PT result plus a polynomial background as the input $\text{Im}_L T$, i.e.:

$$\text{Im}_L T(s) = \text{Im}_L T^{(1)}(s) + \text{Im}_L \left[\frac{a + bs}{\sqrt{s}} \right], \quad (44)$$

where a and b are simply two free parameters without relating to resonance parameters anymore. The fit gives $N(s_0) = 0.57$, $a = -2.39$ GeV and $b = -6.27$ GeV $^{-1}$, and one second sheet pole is found with $\sqrt{s} = 0.95 - 0.25i$ GeV without sizable spurious branch cut contributions.

Since the mass of the ρ meson is fixed we also tried the case of $\mathcal{O}(p^1)$ χ PT results plus the ρ meson exchange term and a polynomial. That is,

$$\text{disc } T(s) = \text{disc } T^{(1)}(s) + \text{disc } T^\rho(s) + \text{disc} \left[\frac{a + bs}{\sqrt{s}} \right]. \quad (45)$$

In this case the ρ meson exchange produces an extra arc in s plane [9], see Fig. 4. We get

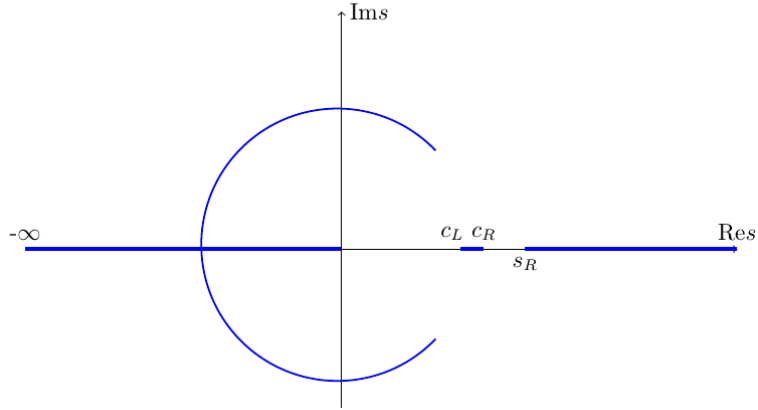


Figure 4: The *l.h.c.* caused by t -channel ρ meson exchange (circular arc [9]); u -channel exchange (line segment from c_L to c_R). The branch point d satisfies $|d| = m_N^2 - m_\pi^2$ [9]

$N(s_0) = 0.61$, $a = -7.88$ GeV, $b = -8.00$ GeV $^{-1}$, and one second sheet pole is found located at

$$\sqrt{s} = 0.90 - 0.20i \text{ GeV}. \quad (46)$$

These solutions are not stable – there exist other solutions but with similar behaviours. In all cases the contributions from the spurious branch cuts are negligible as comparing with the results from the $\mathcal{O}(p^2)$ case, and the $N^*(890)$ pole location remains stable. It is noticed that the contribution from the arc cut generated by t -channel ρ exchange is very small, e.g., it only contributes 1.5° at $\sqrt{s} = 1.16$ GeV.

The “spectral” function in this case is plotted in Fig. 5. Different contributions to the phase shift according to the PKU decomposition are plotted in Fig. 6.

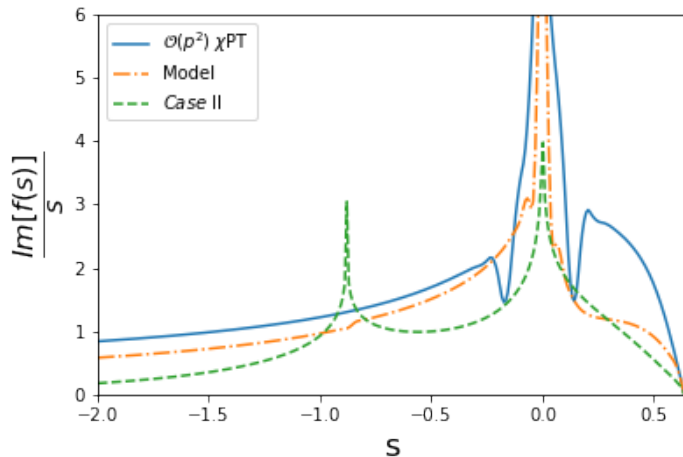


Figure 5: Comparison among different “spectral” functions. The singular behaviors of $T(s)$ at $s = 0$ are $\mathcal{O}(s^{-5/2})$, $\mathcal{O}(s^{-1/2})$ and $\mathcal{O}(s^0)$ for $\mathcal{O}(p^2)$ χ PT, model Eq. (45) and *Case II*, respectively.

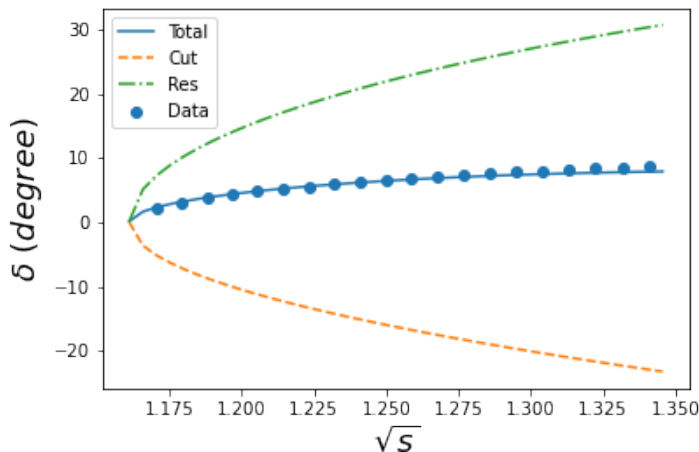


Figure 6: Fit results using Eq. (45). Phase shift decomposition: only contributions from physical ingredients are plotted including their summation ‘Total’. It clearly demonstrates that spurious contributions cancel each other, otherwise curve ‘Total’ cannot get close to the data.

Before closing the discussions on numerical calculations we would like to stress that major physical outputs rely very little on the choice of the cutoff parameter $\Lambda_R^2 = 1.48\text{GeV}^2$. For example, setting $\Lambda_R^2 = 2.0, 2.5\text{GeV}^2$ in model Eq. (45), lead to almost the same pole location at $\sqrt{s} = 0.897 - i0.193\text{GeV}$.

In above, we have made a rather long and exhaustive analyses which has to be stopped somewhere with some regrets. One is that all the calculations made in this paper are performed at tree level only. At loop level, there are of course dynamical cut contributions, like the circular cut. The latter is estimated in Ref. [1] using the complete $\mathcal{O}(p^3)$ χ PT input and it is found that the sign of the circular cut contribution may vary depending on the choice of cutoff parameter, but always remains small in magnitude: e.g., at $\sqrt{s} = 1.16\text{ GeV}$ its contribution to the phase shift is 0.2° when $s_c = 0.32\text{ GeV}^2$, and -1.7° when $s_c = -0.08\text{ GeV}^2$. Since when evaluating the circle there is no problem like what happens at $s = 0$, we think this estimation on the smallness of the circular cut contribution is at least qualitatively reasonable. See Fig. 7, the cutoff parameter $s_c = 0.32\text{GeV}^2$ corresponds to evaluating the *l.h.c.* region covered by the green dashed circle, which can be estimated by chiral perturbation theory; whereas $s_c = -0.08\text{GeV}^2$ corresponds to that covered by the red dotted circle, which is required by best fit. The estimations made in

Refs. [1] [3] pointed out that the region where χ P.T calculation can be safely used is not enough to generate the $N^*(890)$,⁸ i.e., certain help from the contribution in the region $s \in (-\infty, 0.32)$ is needed.⁹ The singularity in the “spectral” function at $s = 0$ seems to be helpful. It is realised that the rescue task is easily fulfilled by looking at Fig. 5. The fit Case II only contains a weak singularity at $s = 0$, i.e., $T(0) \propto \text{const}$ while its contribution in the segment $(0.32, s_L]$ is much weaker than the $\mathcal{O}(p^2)$ ones, but it still affords a pole. The real situation should be much more optimistic. It is noticed that the model Eq. (44) behaves quite like $\mathcal{O}(p^2)$ χ P.T results in the

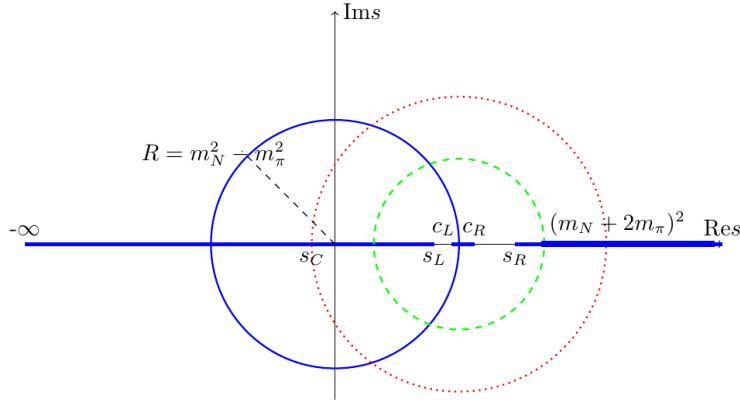


Figure 7: Region of *l.h.c.* being used in Ref. [1]. The cutoff parameter $s_c = 0.32\text{GeV}^2$ corresponds to evaluating the *l.h.c.* region covered by the green dashed circle, which can be estimated by chiral perturbation theory; whereas $s_c = -0.08\text{GeV}^2$ corresponds to that covered by red dotted circle, which is required by best fit.

region $(0.32, s_L)$ and it is expected continuously to work in the region $(-\Lambda_L^2, -\epsilon) \cup (+\epsilon, 0.32)$, where Λ_L^2 is estimated to be around $R = m_N^2 - m_\pi^2$ for example. We make a test by setting $\epsilon \simeq 0.05 \text{ GeV}^2$ and cut off the peak around $s = 0$ in the ‘spectral’ function when $s \in (-\epsilon, +\epsilon)$. The $N^*(890)$ emerges stubbornly with a location $\sqrt{s} = 0.89 - 0.24i \text{ GeV}$.

Hence, we conclude that the *l.h.c.* contributions in total to the phase shift is sizable, based on which the $N^*(890)$ survives with a rather stable pole location. Considering the level of accuracy of our calculations, we do not try to give statistical error bars here in this paper.

5 Discussions and conclusions

It may be somewhat amazing to claim something new in a field under extensive studies for more than half a century. However, according to our studies, a subthreshold broad resonance has well chance of being existed if the *s*-wave phase shift steadily rise above the threshold as a convex curve. The discussion made in the end of the last section suggests that the kinematical singularity structure at $s = 0$ plays a rather important role. This is not surprising. One even finds examples in extreme cases that a pole can be generated totally for kinematic reasons. For example, in $J = 0, I = 2$ channel of $\pi\pi$ scatterings, there exists a virtual pole which can be understood from pure kinematical reasons and it brings important contributions to the phase shift [6], and can be proved to exist rigorously [32]. Another example is the companionate virtual state of the nucleon, which can also be explained for pure kinematical reasons [3].

It is also interesting to notice that the $N^*(890)$ state may be related to the lowest lying $1/2^-$ baryon states suggested by Azimov dated back in 1970 [33] named as N' there, having been searched for desperately since then [34]. Contrary to the original proposal that the lowest lying nucleon counterpart lie above the πN threshold, or at least lie above the nucleon mass (on the 1st sheet), the pole position named $N^*(890)$ determined in Refs. [1] [2] [3] as well as in this

⁸More precisely, the pole position is not stable. For example when taking $s_c = 0.32 \text{ GeV}^2$ the $N^*(890)$ degrades into two deep virtual poles.

⁹Taking $s_c = 0.32 \text{ GeV}^2$ will cause disasters in other channels as well [1].

paper, easily escapes of all bounds and limits set up previously [34]. The mass (width) difference may be explained by a familiar mechanism that when a strong coupling gradually be turned on, the pole will move from the real axis above the threshold to the left of s plane off the real axis. Nevertheless, it may also be possible that the $N^*(890)$ ‘resonance’ be a virtual pole on k plane, as already suggested in Ref. [3]. In the latter situation, the ‘width’ of $N^*(890)$ does not need to have any relations with particle decays. There still remains a lot of work to be done to identify N' and $N^*(890)$. We plan to investigate this question in future.

The N/D calculations discussed in this paper are of rather complicated dynamical ones, however the production representation has been shown to be useful in providing us a simple and pictorial way of understanding the essence of the N/D calculations: in the language of this work, the evidence on the existence of $N^*(890)$ seems to be partly from the peculiar singularity structure of the background integral defined in Eqs. (10). It reads that if $T(s=0)$ does not vanish (or does not vanish fast enough), then an s -wave subthreshold resonance exist, in the most attractive channels.¹⁰ This may even be a rather universal phenomenon, if the background contributions are universally negative, as suggested by quantum scattering theory [36] and repeatedly verified by calculations in quantum field theories. [7] [4] [6]

It is apparent that the existence of a light $1/2^-$ nucleon state is crucial for the completion and establishment of the lowest lying $1/2^-$ octet baryons as suggested in Ref. [33], if ever it exists¹¹. It will definitely improve our understanding of strong interaction physics as well. For example, the $N^*(890)$ state, if exists, will definitely force us to rethink the possible physics behind $f_0(500)$ and $K(700)$. Another question it raises is how to interpret spontaneous chiral symmetry breaking more properly. The textbook explanation on this point is that the axial charge Q_A commutes with the strong interaction hamiltonian, hence if chiral symmetry were not broken parity doublets would appear in nature. But what was observed as the lowest lying $1/2^-$ nucleon is $N^*(1535)$, the non-degeneracy of its mass comparing with the nucleon mass therefore indicates that chiral symmetry is spontaneously broken. The emergence of $N^*(890)$ may also bring new thinking on the related physics.

Finally, it is also pointed out in this paper, that there exist two virtual poles located on the real axis, outside but very close to the u channel cut $[c_L, c_R]$. Their existence is proven relying on the validity of chiral expansions up to all orders.

The authors would like to thank Zhi-hui Guo and De-Liang Yao for helpful discussions at various stage of this work, and Ulf-G. Meißner for a careful reading of the manuscript and useful suggestions. Especially we thank Igor Strakovsky at George Washington University, for very interesting information on the $1/2^-$ octet baryons. This work is support in part by National Nature Science Foundations of China under contract number 11975028 and 10925522, and by the Deutsche Forschungsgemeinschaft (DFG, German Research Foundation) - Project-ID 196253076 -TRR 110.

Reference

- [1] Y. F. Wang, D. L. Yao, and H. Q. Zheng, *Chin. Phys. C* **43**, 064110 (2019).
- [2] Y. F. Wang, D. L. Yao, and H. Q. Zheng, *Front. Phys. (Beijing)* **14**, 24501 (2019).
- [3] Y. F. Wang, D. L. Yao, and H. Q. Zheng, *Eur. Phys. J. C* **78**, 543 (2018).
- [4] H. Q. Zheng *et al.*, *Nucl. Phys. A* **733**, 235 (2004).
- [5] Z. Y. Zhou and H. Q. Zheng, *Nucl. Phys. A* **775**, 212 (2006).
- [6] Z. Y. Zhou *et al.*, *JHEP* **02**, 043 (2005).
- [7] Z. G. Xiao and H. Q. Zheng, *Nucl. Phys. A* **695**, 273 (2001).
- [8] J. Y. He, Z. G. Xiao, and H. Q. Zheng, *Phys. Lett. B* **536**, 59 (2002), [Erratum: *Phys. Lett. B* 549, 362–363 (2002)].

¹⁰Similar observations are obtained, from a different point of view. [35].

¹¹For more information on the status of the octet baryons, see the talk of Igor Strakovsky given at *EHS – 2019*, York, UK, December 2019.

- [9] Y. Ma, W. Q. Niu, Y. F. Wang, and H. Q. Zheng, *Commun. Theor. Phys.* **72**, 105203 (2020).
- [10] Y. Ma, W. Q. Niu, D. L. Yao, and H. Q. Zheng, *Chin. Phys. C* **45**, 014104 (2021).
- [11] X. H. Cao, Y. Ma, and H. Q. Zheng, *Phys. Rev. D* **103**, 114007 (2021).
- [12] D. L. Yao, L. Y. Dai, H. Q. Zheng, and Z. Y. Zhou, *Rep. Prog. Phys.* **84**, 076201 (2021).
- [13] A. Gasparyan and M. F. M. Lutz, *Nucl. Phys. A* **848**, 126 (2010).
- [14] J. Kennedy and T. D. Spearman, *Phys. Rev.* **126**, 1596 (1961).
- [15] M. Hoferichter, J. Ruiz de Elvira, B. Kubis, and U.-G. Meißner, *Physics Reports* **625**, 1 (2016).
- [16] J. M. Alarcon, J. Martin Camalich, and J. A. Oller, *Annals Phys.* **336**, 413 (2013).
- [17] Y. H. Chen, D. L. Yao, and H. Q. Zheng, *Phys. Rev. D* **87**, 054019 (2013).
- [18] P. C. Bruns, M. Mai, and U. G. Meißner, *Phys. Lett. B* **697**, 254 (2011).
- [19] D. Siemens *et al.*, *Phys. Rev. C* **94**, 014620 (2016).
- [20] D. Siemens *et al.*, *Phys. Lett. B* **770**, 27 (2017).
- [21] D. Siemens *et al.*, *Phys. Rev. C* **96**, 055205 (2017).
- [22] H. P. Jakob and F. Steiner, *Z. Phys.* **228**, 353 (1969).
- [23] M. Hoferichter, J. Ruiz de Elvira, B. Kubis, and U.-G. Meißner, *Phys. Rev. Lett.* **115**, 192301 (2015).
- [24] D. L. Yao *et al.*, *JHEP* **05**, 038 (2016).
- [25] S. Scherer and M. R. Schindler, *A primer for chiral perturbation theory*, Vol. 830 (Springer Science & Business Media, 2011).
- [26] J. J. Sanz-Cillero, D. L. Yao, and H. Q. Zheng, *Eur. Phys. J. C* **74**, 2763 (2014).
- [27] G. Y. Qin, W. Z. Deng, Z. Xiao, and H. Q. Zheng, *Phys. Lett. B* **542**, 89 (2002).
- [28] G. Ecker, J. Gasser, A. Pich, and E. de Rafael, *Nucl. Phys. B* **321**, 311 (1989).
- [29] V. Bernard, N. Kaiser, and U.-G. Meissner, *Nucl. Phys. A* **615**, 483 (1997).
- [30] T. Appelquist and J. Carazzone, *Phys. Rev. D* **11**, 2856 (1975).
- [31] B. A. Ovrut and H. J. Schnitzer, *Phys. Rev. D* **22**, 2518 (1980).
- [32] Z. H. Guo, J. J. Sanz-Cillero, and H. Q. Zheng, *JHEP* **06**, 030 (2007).
- [33] Y. I. Azimov, *Phys. Lett. B* **32**, 499 (1970).
- [34] Y. I. Azimov, R. A. Arndt, I. I. Strakovsky, and R. L. Workman, *Phys. Rev. C* **68**, 045204 (2003).
- [35] Z. Xiao and Z.-Y. Zhou, *Phys. Rev. D* **94**, 076006 (2016).
- [36] T. Regge, *Nuovo Cim.* **8**, 671 (1958).

A Phenomena of the cut $[c_L, c_R]$ induced by u channel nucleon exchanges

The u channel nucleon pole exchange diagram will contribute to the partial wave amplitude a cut $\in [c_L, c_R]$, with $c_L = \frac{(m_N^2 - m_\pi^2)^2}{m_N^2}$ and $c_R = m_N^2 + 2m_\pi^2$. The point $s = c_L$ is reached when $z_s = -1$, $u = m_N^2$ and $s = c_R$ is reached when $z_s = +1$, $u = m_N^2$ (see Eq. (27)). More precisely, at branch points c_L and c_R one gets the leading term of the partial wave amplitude:

$$\begin{aligned} s \rightarrow c_L : \quad T(s) &\rightarrow -\frac{g^2 m_N^4}{16\pi F^2 (4m_N^2 - m_\pi^2)} \ln \frac{s - c_L}{c_L - c_R}, \\ s \rightarrow c_R : \quad T(s) &\rightarrow \frac{g^2 m_N^2 (m_N^2 + 2m_\pi^2)}{\pi F^2 (4m_N^2 - m_\pi^2)} \ln \frac{c_R - c_L}{s - c_R}, \end{aligned} \quad (47)$$

which are solely from the u channel nucleon pole term, and are hence exact, i.e., receiving no chiral corrections. Based on Eq. (47) one further finds

$$\begin{aligned} s \rightarrow c_L, \quad S &\simeq A_{c_L} + B_{c_L} \ln \frac{s - c_L}{c_L - c_R}, \\ s \rightarrow c_R, \quad S &\simeq A_{c_R} + B_{c_R} \ln \frac{s - c_R}{c_R - c_L}, \end{aligned} \quad (48)$$

in which the coefficients read

$$\begin{aligned} A_{c_L} = A_{c_R} &= 1 + \frac{g^2 m_N m_\pi}{8\pi F^2} + O(m_\pi^3), \\ B_{c_L} = B_{c_R} &= \frac{g^2 m_N m_\pi}{16\pi F^2} + O(m_\pi^3). \end{aligned} \quad (49)$$

These equations are obtained from Born term calculations, A_{c_L} (B_{c_L}) and A_{c_R} (B_{c_R}) differ at $O(m_\pi^3)$ level. It is worth emphasizing that A_{c_L} and A_{c_R} may receive chiral corrections, but B_{c_L} and B_{c_R} do not, since the latter is related to the residue of the u channel nucleon pole.

One important conclusion one can draw is that $S(c_L), S(c_R) \rightarrow -\infty$ which are exact (correct at least to any order of chiral expansions) and are immune of any loop corrections. Remember that $S = +1$ at s_L and s_R by definition, and $S(s)$ is real when $s \in (s_L, c_L) \cup (c_R, s_R)$, one finds that there have to be two S matrix zeros: one below c_L and another above c_R , on the real axis.¹² Their locations (denoted by v_L and v_R) are:

$$\begin{aligned} v_L &= c_L - (c_R - c_L)e^{-A_{c_L}/B_{c_L}}, \\ v_R &= c_R + (c_R - c_L)e^{-A_{c_R}/B_{c_R}}. \end{aligned} \quad (50)$$

Even more surprisingly, these two virtual poles in total give a large contribution to the phase shift. E.g., they give roughly 50° at $\sqrt{s} = 1.16\text{GeV}$, which seems to completely destroy the picture presented in Figs. 3 and 6. The solution to this apparent paradox is rather tricky, which we discuss in the following.

In the derivation of the production representation, Eqs. (10) and (12), it is generally assumed that the branch cut singularity structure of $S^{cut} (= \exp\{2i\rho(s)f(s)\})$ and $f(s)$ (or $\ln S^{cut}$) being the same. This is not always being true: when S^{cut} is real and negative at certain point, $\ln S^{cut}$ will have to be discontinuous when the sign of the imaginary part of S^{cut} changes. This situation indeed happens in the present situation. Recall that at $O(p^1)$ level

$$\begin{aligned} T^{(1)} &= -\frac{g^2 (-2m_N^2 m_\pi^2 - m_N^2 s - m_\pi^2 s + s^2)}{32\pi F^2 (s - m_N^2)} + \frac{-m_N^2 - m_\pi^2 + s}{32\pi F^2} \\ &+ \frac{m_N (-m_N^2 + m_\pi^2 + s)}{32\pi F^2 \sqrt{s}} - \frac{g^2 m_N (-m_N^4 + m_N^2 m_\pi^2 + m_N^2 s + 2m_\pi^2 s)}{32\pi F^2 (s - m_N^2) \sqrt{s}} \\ &+ \frac{g^2 m_N^2 s^2 (-m_N^2 - m_\pi^2 + s)}{16\pi F^2 (s - c_L)^2 (s - c_R)^2} \left(\frac{m_N^2}{s} (s - c_L) \left(\log \frac{s - c_L}{s - c_R} + \log \frac{m_N^2}{s} \right) - s\rho(s)^2 \right) \\ &- \frac{g^2 m_N^3 s^2 (-m_N^2 + m_\pi^2 + s)}{16\pi F^2 (s - c_L)^2 (s - c_R)^2 \sqrt{s}} \left((s - c_R) \left(\log \frac{s - c_L}{s - c_R} + \log \frac{m_N^2}{s} \right) - s\rho(s)^2 \right). \end{aligned} \quad (51)$$

¹²In a K -matrix unitarization, the S matrix no longer diverges at $s = c_L, c_R$, the two virtual poles however still exist, and no major conclusions change.

It is seen from the above expressions that the cut $L \in (-\infty, 0) \cup (c_L, c_R)$. There are two sources contributing to the imaginary part of $T(s)$ when $s \in (-\infty, 0)$: one comes from the kinematical \sqrt{s} while another comes from the logarithmic function; when $s \in (c_L, c_R)$ $\text{Im}T$ solely comes from the u channel nucleon pole exchange. On (c_L, c_R) the imaginary part of $T^{(1)}$ reads:

$$\begin{aligned} \text{Im}T^{(1)}(s) &= \frac{g^2 m_N^2 s^2}{16F^2 (s - c_L)^2 (s - c_R)^2} \\ &\times \left[\frac{m_N^2}{s} (s - c_L) (-m_N^2 - m_\pi^2 + s) - \frac{m_N}{\sqrt{s}} (s - c_R) (-m_N^2 + m_\pi^2 + s) \right], \end{aligned} \quad (52)$$

from which it is seen that the $\text{Im}T^{(1)}$ develops a zero at $s = s_c \simeq m_N^2 - \frac{m_\pi^4}{2m_N^2}$ and changes sign when s crosses s_c . It is important to realize that Eq. (52) is immune of chiral perturbation corrections.

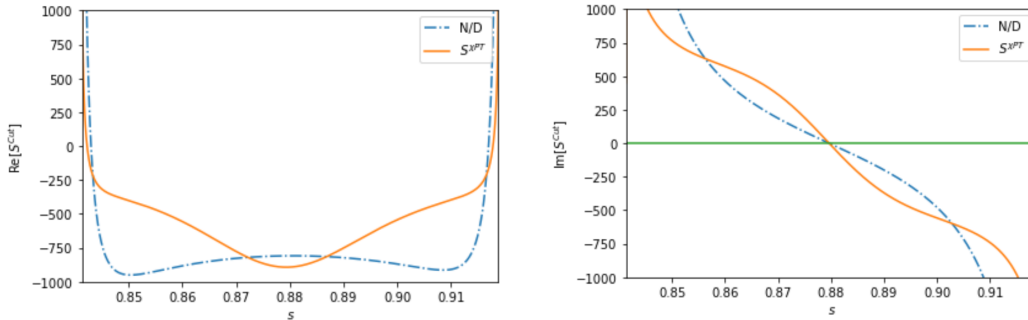


Figure 8: Real (left) and imaginary (right) part of $S^{cut}(s)$ when s lies in (c_L, c_R) . The dot-dashed line comes from N/D solution of Eq. (44), the yellow solid line is obtained from $O(p^1)$ χ PT results.

From Fig. 8, it is found that the imaginary part of S^{cut} vanishes at one point s_c which is close to m_N^2 meanwhile the real part of S^{cut} is negative. In Fig. 8 S^{cut} is calculated by

$$S^{cut} = \frac{S^{phys}}{\prod_p S^p \times S^{v_L} \times S^{v_R}} \quad (53)$$

where the newly found virtual poles are included, and S^{phys} are approximated by both the unitary amplitude obtained by fitting Eq. (44) and the pure $O(p^1)$ perturbation amplitude.¹³ From Fig. 8 it is seen that at $s = s_c$, $\ln S^{cut}$ has to develop a discontinuity and hence a branch cut emerges crossing s_c . It is numerically checked that the cut is an arc on the complex s -plane in N/D solutions. It should be emphasized here that this unexpected additional cut does not pollute S^{cut} , since across the cut the discontinuity of $\ln S^{cut}$ is $2i\pi$ and has no influence to the value of an exponential. Though not producing any trouble in the analyticity structure of S^{cut} , the additional cut of $\ln S^{cut}$, or the dispersive representation of function f defined in Eq. (10) has to be changed since the integration contour has to be modified.

The problem found above is rather severe since the distorted contour may depend on numerics and hence being impossible to control. However, it can be overcome by the following consideration. Define

$$\bar{f}(s) = \frac{\ln -S^{cut}}{2i\rho(s)} - \frac{\pi}{2\bar{\rho}(s)} \quad (54)$$

where the function $\bar{\rho}(s)$ is the ‘deformed’ $\rho(s)$ with its cut $\in [s_L, s_R]$, while the cut of the latter is defined on $(-\infty, s_L] \cup [s_R, +\infty)$. Notice that $\bar{\rho}(s)$ and $\rho(s)$ are identical in the physical region. Function $\bar{f}(s)$ is identical to $f(s)$ when s in the physical region as well but differs in cut alignment. Particularly \bar{f} no longer contains the arc cut of f , since s_c is not a branch point of \bar{f} anymore. However, \bar{f} contains an additional cut induced by $\bar{\rho}$ which is absent in f . Both the

¹³The ‘ $O(p^1)$ calculation’ in Fig. 8 is done via Eq. (53) in the following way: S^{phys} is calculated in $O(p^1)$, ‘poles’ are picked up by searching for zeros of S^{phys} , though they are actually not second sheet poles for lacking of unitarity.

two terms on the *r.h.s.* of Eq. (54) contain cuts on $[s_L, s_R]$, but the two cuts cancel each other when $s \in [c_R, s_R]$. Hence the left cut of \bar{f} on the real axis is actually $[-\infty, c_R]$, comparing with the left cut of f on the real axis: $[-\infty, s_L] \cup [c_L, c_R]$. The dispersive integral representation of \bar{f} can be written as:

$$\begin{aligned} \bar{f}(s) = & \frac{s}{\pi} \int_L \frac{\text{Im}[\ln -S^{cut}(s')/(2i\rho(s'))]}{s'(s'-s)} ds' \\ & + \frac{s}{\pi} \int_{s_L}^{c_L} \frac{\text{Im}[\ln -S^{cut}(s')/(2i\rho(s'))]}{s'(s'-s)} ds' \\ & - s \int_{s_L}^{c_R} \frac{\text{Im}[1/(2\bar{\rho}(s'))]}{s'(s'-s)} ds' . \end{aligned} \quad (55)$$

In the first term on the *r.h.s.* of the above equation, the integration domain $L = (-\infty, s_L] \cup [c_L, c_R]$, i.e., the same as that in Eq. (10). Actually the first term is identical to f defined in Eq. (10) as in the integrand S^{cut} can actually be replaced by S^{phys} . To prove this it is realized that, firstly, on $(-\infty, s_L]$, $\text{Im}[\ln -S^{cut}/(2i\rho)] = -\ln |S^{cut}|/(2\rho)$, and $|S^{cut}| = |S^{phys}|$. Secondly, the integral on $[c_L, c_R]$ can be recast as

$$\begin{aligned} \frac{s}{\pi} \int_{c_L}^{c_R} \frac{\text{Im}[\ln -S^{cut}(s')/(2i\rho(s'))]}{s'(s'-s)} ds' &= \frac{s}{2i\pi} \int_{c_L}^{c_R} \frac{\ln[S_+^{cut}/S_-^{cut}]}{2i\rho(s')s'(s'-s)} ds' \\ &= \frac{s}{2i\pi} \int_{c_L}^{c_R} \frac{\ln[S_+^{phys}/S_-^{phys}]}{2i\rho(s')s'(s'-s)} ds' = \frac{s}{\pi} \int_{c_L}^{c_R} \frac{\text{Im}[\ln S^{phys}(s')/(2i\rho(s'))]}{s'(s'-s)} ds' , \end{aligned} \quad (56)$$

where $S_{\pm} \equiv S(s \pm i\epsilon)$. Hence we complete the proof.

The second integral in Eq. (55) is analytically integrable once it is realized that S^{cut} is positive definite along $[s_L, c_L]$, and the third integral is also integrable. The sum of the two integrals gives a contribution to the phase shift exactly canceled by the contribution from the two virtual poles, when their positions are taken at c_L and c_R . If the two virtual pole locations are fixed by Eq. (50), the net effects of the sum of virtual poles and the additional cut are vanishingly small (e.g., of order of 10^{-3} degrees at $\sqrt{s} = 1.16\text{GeV}$). Therefore, The calculation using Eq. (10) is still valid with high accuracy, when one ignores the existence of the two virtual poles. Further, it is worth emphasizing that after such a surgery, there no longer exists the unwanted cut in $\ln S^{cut}$ crossing s_c , as checked by numerical analyses. Moreover, it may be worth pointing out that in numerical analyses there may appear additional cuts in $\ln S^{cut}$ as well on the s plane in distance, which is caused by the peculiar analyticity property of the logarithmic function. But it is easy to prove that it is not hazardous and can be simply ignored.

The discussions made in this appendix can be extended to higher partial waves as well and some very interesting results appear, which will be presented elsewhere.